

Article

Mechanical Alloying Process Applied for Obtaining a New Biodegradable Mg-xZn-Zr-Ca Alloy

Doina Raducanu ¹, Vasile Danut Cojocaru ^{1,*} , Anna Nocivin ², Radu Hendea ³, Steliana Ivanescu ³, Doina Stanciu ³ , Corneliu Trisca-Rusu ⁴, Silviu Iulian Drob ⁵ and Elisabeta Mirela Cojocaru ¹

- ¹ Department of Metallic Materials Processing and Ecometallurgy, University POLITEHNICA of Bucharest, 060042 Bucharest, Romania; doina.raducanu@upb.ro (D.R.); mirela.cojocaru@upb.ro (E.M.C.)
- ² Faculty of Mechanical, Industrial and Maritime Engineering, Ovidius University of Constanta, 900527 Constanta, Romania; anocivin@univ-ovidius.ro
- ³ Zircon Dent Srl, 400690 Cluj-Napoca, Romania; office@zircon-dent.com (R.H.); sivanescu@yahoo.com (S.I.); doinastanciu09@yahoo.com (D.S.)
- ⁴ National Institute for Research and Development in Micro-Technologies, 077190 Bucharest, Romania; corneliu.trisca@nano-link.net
- ⁵ Romanian Academy, Institute of Physical Chemistry “Ilie Murgulescu”, Splaiul Independentei 202, 060021 Bucharest, Romania; sidrob.icf@gmail.com
- * Correspondence: dan.cojocaru@upb.ro

Abstract: The aim of the present paper is to apply the mechanical alloying process to obtain from powder components a new biodegradable Mg-based alloy powder from the system Mg-xZn-Zr-Ca, with high biomechanical and biochemical performance. Various processing parameters for mechanical alloying have been experimented with the ultimate goal to establish an efficient processing route for the production of small biodegradable parts for the medical domain. It has been observed that for the same milling parameters, the composition of the powders has influenced the powder size and shape. On the other hand, for the same composition, the highest experimented milling speed and time conduct to finer powder particles, almost round-shaped, without pores or various inclusions. The most uniform size has been obtained for the powder sample with 10 wt.%Zn. These powders were finally processed by selective laser melting, an additive manufacturing technology, to obtain a homogeneous experimental sample, without cracking, for future more systematical trials.

Keywords: magnesium alloy; mechanical alloying; microstructure; power morphology



Citation: Raducanu, D.; Cojocaru, V.D.; Nocivin, A.; Hendea, R.; Ivanescu, S.; Stanciu, D.; Trisca-Rusu, C.; Drob, S.I.; Cojocaru, E.M. Mechanical Alloying Process Applied for Obtaining a New Biodegradable Mg-xZn-Zr-Ca Alloy. *Metals* **2022**, *12*, 132. <https://doi.org/10.3390/met12010132>

Academic Editor: Petra Maier

Received: 7 December 2021

Accepted: 6 January 2022

Published: 11 January 2022

Publisher's Note: MDPI stays neutral with regard to jurisdictional claims in published maps and institutional affiliations.



Copyright: © 2022 by the authors. Licensee MDPI, Basel, Switzerland. This article is an open access article distributed under the terms and conditions of the Creative Commons Attribution (CC BY) license (<https://creativecommons.org/licenses/by/4.0/>).

1. Introduction

Between biodegradable metals, such as Fe, Mg and Zn used for human temporary implants, magnesium is the most appreciated because it has higher biocompatibility compared to its counterparts and also the mechanical properties are closest to human bone [1,2]. Magnesium, apart from its proven osteoconductive role and significant facilitating of the bone cellular ingrowth, has a density of just 1.74 g/cm³, being lighter than Fe and Zn with about 4.5 and 4.1 times respectively, and with about 2.6 times than titanium, another widely used biomaterial. Thus, Mg has the closest density to that of natural bone (1.8–2.1 g/cm³). Concerning Young's modulus, also an important characteristic related to medical applications, Mg alloys show lower values than commonly used titanium alloys (41–45 GPa comparative to 55–110 GPa) [3–5]. The numerous published scientific reports for the last decade show the high interest in this metal and its alloys, with a successful application for clinically proven biodegradable metal scaffolds [6,7] or bone screws [7–9]. A useful application refers to bone grafting for promoting bone repair in case of large bone trauma, for which the Mg metal/alloy being biodegradable presents important advantages because the Mg ion manifests a positive effect for initiating bone regeneration [2,10]. Ti alloys, with their large use for biomedical bone implants, are not biodegradable unfortunately.

They can promote bone growth because Ti alloys can transfer mechanical stimuli to the bone, withstanding stress, but they cannot be absorbed, remaining as barriers in bone reconstruction. [10]. However, for biodegradable Mg metal/alloy, the main difficulty is represented by the manufacturing of porous scaffolds with particular and suitable macro or micro geometry adapted exactly to the anatomy of the patient from point of view of the pore's morphology design and control [2]. From this perspective, the classical methods, such as sintering, foaming, or chemical vapor deposition have been proven to be inefficient for obtaining the necessary interconnected pores with suitable morphology and quantity to initiate cell ingrowth [11–13]. The additive manufacturing (AM) methods come in last years to successfully overcome this problem knowing that a geometric complex structure is impossible to achieve using conventional manufacturing methods even if metal-3D-printers are expensive and do not allow the manufacture of large parts in mass production but only of particular geometries adapted on the patient.

Till now, the only metal implants made by AM and clinically proved are from non-degradable metals, mainly Ti alloys [14–16]. However, as an ideal implant involves biodegradation, the application of AM for obtaining implants with this function becomes a necessity, and therefore, the development of such a technology on Mg alloys is of the utmost relevance and actuality.

The AM methods, that imply metallic powder bed fusion, can use electron-beam (EB-PBF), but most frequently laser (L-PBF) with more recent and adapted names, such as selective laser melting (SLM). The EB-PBF method is not suitable for Mg alloys due to the evaporation of the Mg that affects the propagation of an electron beam in the vacuum [17–19]. For the SLM method two actions are most important for a successful result: first, the obtaining of the metallic powder with desired chemical composition, dimension and morphology, as fine as possible; secondly, the selection of the laser parameters (power, spot size, spot speed, energy density) that assure good final results. The metallic powder should be as fine as possible to assure the best concordance between designed geometry and as-built geometry. For that objective, the powders should be of spherical shape, uniform size and high density, meaning without pores, or various inclusions, such as defects [1,2]. These kinds of metallic powders are often produced by gas atomization. Water atomization is another possible method, but the metallic powder results in an irregular shape and a greater oxygen content, which affects further SLM processing [1,2]. A third possibility is mechanical alloying (MA) which represents one of the most efficient and low-cost modalities to obtain/produce metallic powders with fine microstructures and dimensions [20–22].

Regarding the chemical composition, the Mg alloys for the medical domain can be alloyed with chemical elements, such as Zn, Zr, Ca, Sr, Si or rare earth (RE) elements, such as Nd, Y, Gd, Sc, that besides being biocompatible, can also improve the mechanical properties and corrosion resistance of the Mg [23]. The entire processing of these alloys is hindered by severe evaporation and high chemical reactivity of the Mg. Till now, there are some scientific reports regarding several biodegradable Mg alloys, such as: [17,24] for pure Mg powder; [25] for Mg-Al alloy; [26–30] for Mg-Al-Zn alloy, short-named as AZ; [31] for Mg-Zn-Zr alloy, short-named as ZK; [32,33] for Mg-RE-Zr alloy, short-named as WE; [34] for Mg-Zn-Ca-Gd alloy. All these reports represent only preliminary attempts and refer to either alloys that contain Al, which has been shown to promote neurodegenerative diseases or even cancer [35], or RE elements that are expensive and difficult to access. As concerning mechanical alloying, so far poor information is available concerning the production of Mg alloys in powder state obtained by this approachable technology, mainly due to the high oxygen reactivity of the Mg. Anyway, literature reports suppose that if the technological parameters are well mastered, this method can promote suitable powders with appreciated characteristics [1,21,36].

Therefore, the present study proposes a series of new chemical compositions for a biodegradable alloy based on Mg, intended to be synthesized by mechanical alloying, first, to be further processed by SLM. These new compositions start from Mg-Zn-Zr (ZK) alloy,

but with Ca in plus. All selected alloying elements are biocompatible and affordable; the aim is to obtain a fine powder, with appropriate dimensions and morphology, suitable for further SLM-processing. For this, various processing parameters of MA will be experimented with. The ultimate goal is to establish an efficient MA + SLM processing route for the production of small biodegradable parts for the medical domain. The present study focuses only on finding the appropriate MA processing parameters. Further, SLM attempts will be tested and reported in future studies.

2. Materials and Methods

2.1. The Design/Selection of the New Chemical Composition for the Mg-Zn-Ca-Zr Alloy

For the experimental program, a new alloy of Mg-Zn-Ca-Zr type was selected. The first reason was based on proposing biocompatible elements, other than Al or RE as they have been experimented with before, due to reported medical complications mentioned above [35]. In addition, all proposed alloying elements are biodegradable.

Zinc (Zn), the main alloying element, is relatively inoffensive compared to other metal ions with similar chemical properties. The degradation rate of Zn is situated between those of Mg and Fe, so it represents a good alloying achievement for a biodegradable Mg alloy [37,38]. Zn also plays an essential role in many biological functions in the body and is vital in over 300 metabolic activities of the body's enzymes as well as for cell division, DNA and protein synthesis [39]. Zinc melting can be performed in air, but the tendency to evaporate is much higher than that of Mg, unfortunately. As such, this aspect must be taken into account for the SLM method applied after mechanical alloying. By alloying Mg with Zn, is expected that the tensile strength will increase, according to [40]. For the present experimental program, the selected alloying amount of Zn was tested in three variants —4 wt.%, 6 wt.%, and 10 wt.% —with an increasing quantity of Zn due to its well-known biocompatibility, even if the third composition is over the equilibrium limit of solubility in α -Mg (6.2 wt.% at 340 °C) [31].

Calcium (Ca) is one of the most important chemical elements for human bone, by performing chemical signaling with different cells [41,42]. Calcium, like Mg, has a low density (1.55 g/cm³) being also very close to that of natural bone (1.8–2.1 g/cm³). It is not an expensive alloying element, favoring the production of hydroxyapatite in the body, thereby accelerating bone healing [43,44]. It is also reported that Ca represents an important factor able to control the corrosion rate of Mg alloys [45]. We proposed a new Mg-Zn-Ca-Zr alloy, the selected amount of Ca is 0.8 wt.% for all tested variants, which is under the maximal equilibrium limit of Ca solubility in Mg (1.11 wt.% at 521 °C).

Zirconium (Zr) represents also a known biocompatible and biodegradable chemical element that helps in refining the microstructure of Mg alloys. The selected amount of Zr is 0.5 wt.% for all tested variants, a value which is within the solubility limit in α -Mg.

In conclusion, it results in the following three new compositional variants to be tested, not-experimented before (wt.%): (1) Mg-4Zn-0.8Ca-0.5Zr; (2) Mg-6Zn-0.8Ca-0.5Zr; (3) Mg-10Zn-0.8Ca-0.5Zr.

2.2. The Mechanical Alloying Procedure Applied for Obtaining the Mg-Zn-Ca-Zr Alloy Powder

2.2.1. The Mechanical Alloying Process

For the Mechanical Alloying (MA) process, a ball mill with high energy was necessary through which the collision between the grinding media and the powder particles developed a high energy impact on the charged powder producing severe plastic deformation that implied high impacts, shears and torsional forces [46], repeated fracturing and cold welding of the presented particles; all the phenomena led to the formation of a material with nano-crystalline structure even if the powder shape is more irregular/non-spherical [21,22]. The technology of mechanical alloying involves the loading of pure elementary powders (or pre-alloyed powders) in a mill with high-energy balls representing the grinding medium. Usually, the weight ratio between grinding balls and powder is around 10: 1, or higher [46]. The process implies repeated fracturing, cold welding, re-fracturing and re-welding of

the powder particles. That is the reason why during the mechanical alloying process the size of the resulting powder can be controlled by optimizing/balancing the fracturing and welding processes. For that, when ductile metals are processed, as in the present case, for minimizing the excessive cold welding among powder particles or between them and the milling container and/or grinding medium, a so-named process-control-agent is used usually, for example, 5% n-heptane solution, which can be absorbed on the powder surfaces and decrease the exceeding cold welding; this process can inhibit the powder particle agglomeration. The dimension of the powder particles and their grain sizes decrease gradually with milling time, until the nanometer scale.

2.2.2. The Mechanical Alloying Parameters Used for the Experiments

A mixture of elemental Mg powder (99.00% pure, <math><100\text{--}150\ \mu\text{m}</math>), Zn powder (99.00% pure, <math><50\ \mu\text{m}</math>), Zr powder (99.00% pure, <math><50\ \mu\text{m}</math>) and Ca granules were mechanically milled for various milling times, from 2 to 35 h. Figure 1 shows the experimental scheme of the MA process applied for each of three new compositional variants of studied Mg alloy.

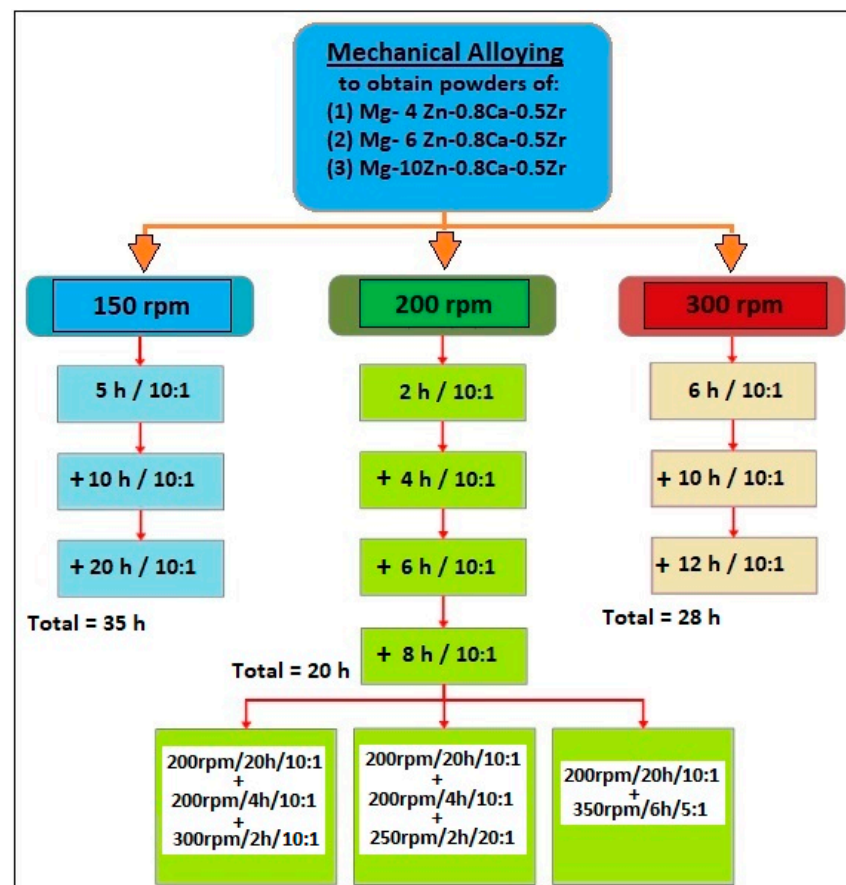


Figure 1. The experimental scheme of mechanical alloying process applied for each of three new compositional variants of studied Mg alloy; various milling speed [rpm]; various milling times [h]; various powder to oxide ball weight ratios.

Mechanical alloying was carried out using a high-energy PM 100 Retsch planetary mill (Retsch-Verder Romania S.R.L., Bucharest, Romania) (500 mL capacity/50/60 Hz frequency/10 mm diameter of zirconium oxide balls) under an argon atmosphere –1.5 bar overpressure; 5% n-heptane solution was added onto the powder mixture prior to the milling process to prevent excessive cold welding of the elemental alloy powders. The powder to oxide ball weight ratio of 10:1 (most frequent), 20:1 (one attempt) and 5:1 (also one attempt) was applied. The milling speed was between 150–350 rpm. After the MA

process, the obtained powders were sieved successively by the following dimensions: (1) 100–60 μm ; (2) 60–30 μm ; (3) <30 μm .

Finally, some of the obtained powders were selected to be processed by the SLM method for finding the most promising MA variants for further SLM trials. For the SLM method, selective amounts of metal powders were melted according to the initial computer-aided design (CAD) process. When the selective melting of the first layer was completed, the support platform was lowered by a certain distance initially set so that the next layer of powder is deposited on this platform and the process continues [18,19]. The type of laser used was MYSINT 100-3D Selective Laser Fusion (SISMA s.p.a., Vicenza, Italy) —printer for metal powder, with power supply 220–240 V, 50/60 Hz; maximum power absorbed 1.53 Kw; inert gas—Nitrogen, Argon. The used processing SLM parameters were: laser power—100–200 W; laser speed—700–1100 mm/s; layer height—20–30 mm; laser energy density—166–578 J/mm³.

2.3. The Microstructural Investigations of the Mg-xZn-Ca-Zr Alloy Powder

Scanning electron microscopy–energy dispersive spectroscopy (SEM-EDS) and scanning electron microscopy–secondary electron (SEM-SE) imaging investigations were performed using a Tescan VEGA II-XMU SEM microscope equipped (Tescan Orsay Holding, a.s., Brno, Czech Republic) with a Bruker QUANTAX xFlash 6/30 EDS detector. This analysis was performed to examine the characteristics of the obtained powders: their consistency, homogeneity, morphology, dimension, cold welding, etc.

Qualitative X-ray diffraction (XRD) analysis was performed to identify the presence of chemical elements and phases only for the most promising variants (close to spheric shape). The conventional X-ray diffraction was carried out at room temperature (RT, 298 K) using a Panalytical X'Pert PRO MRD diffractometer (Malvern Panalytical Ltd., Malvern, UK), with Cu-k α radiation ($\lambda = 0.15418$ nm) in the 2θ range of 30°–90°, using a step size of 0.02°, operating voltage and current of 40 kV and 30 mA, respectively. The recorded XRD patterns were fitted using the PeakFit v4.11 software package (version 4.11, Systat Software Inc., London, UK) to de-convolute the observed cumulative diffraction peaks and to determine, for each constitutive peak, the position, intensity, and broadening FWHM (full width at half maximum).

3. Results and Discussion

In conformity with Figure 1, a large number of experimental MA variants have been applied by varying the processing parameters: the milling speed (150 rpm, 200 rpm, 300 rpm) and the milling number of hours (2–35 h). The ultimate goal was to obtain a powder as fine as possible, with shapes as close as possible to the spherical, with uniform dimensions and without pores or various inclusions as defects.

In this direction, a series of SEM images (Figures 2–9) are presented in the following, showing a selection of obtained powders with various parameters. The most promising variants, as expected, turned out to be those with high value parameters: many milling hours, of about 16–28 h and for high milling speed—300 rpm. Indeed, it can be observed that by increasing both parameters—rotation speed or the number of milling hours—the obtained powders become finer and closer to spherical shape. For example, comparing the powders in Figures 2–4 with those in Figures 8 and 9, it can be seen that the powder size becomes finer and more homogeneous for the same powder composition. Figures 2–9 correspond to powders with a composition of 10% Zn, but the assessments made above are also valid for the other two compositions.

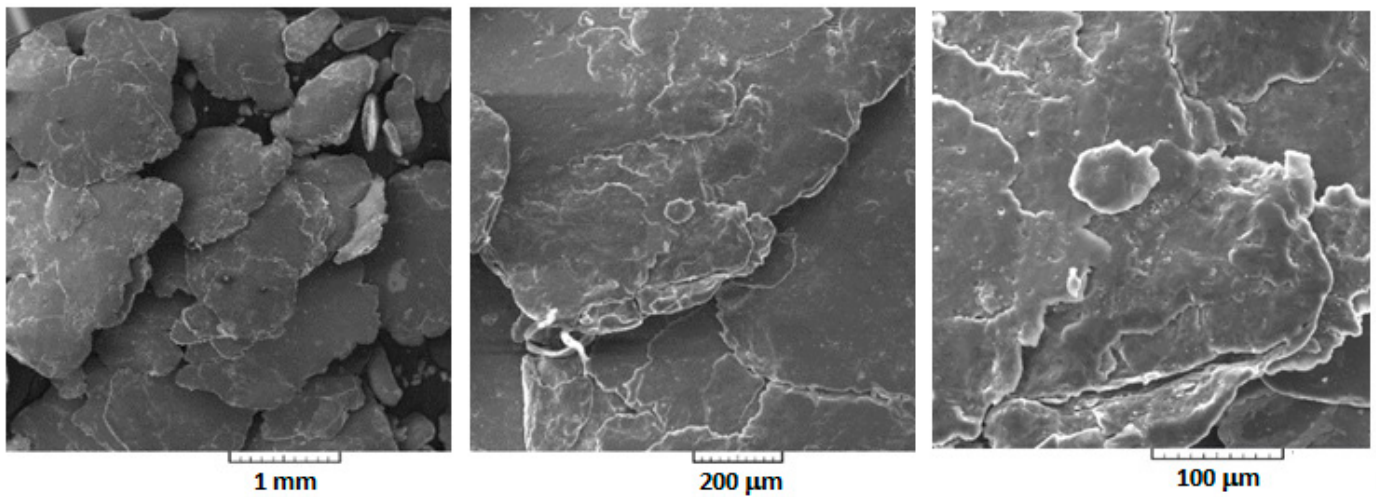


Figure 2. The Mg-10Zn-0.8Ca-0.5Zr (wt.%) alloy-powder was processed by mechanical alloying with 150 rpm/15 h/10:1.

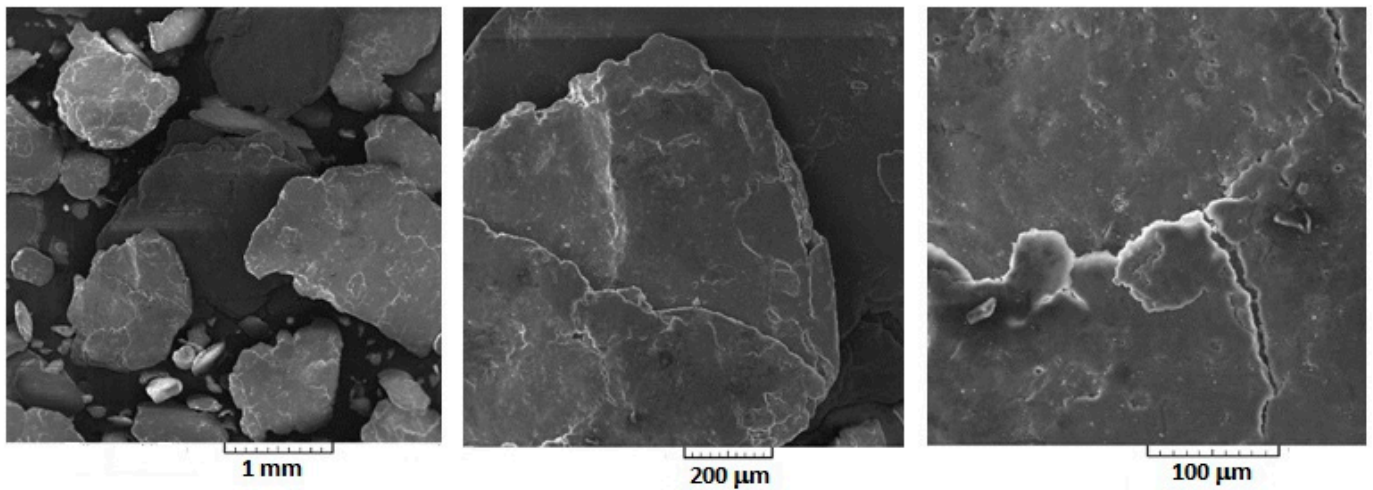


Figure 3. The Mg-10Zn-0.8Ca-0.5Zr (wt.%) alloy-powder processed by mechanical alloying with 150 rpm/35 h/10:1.

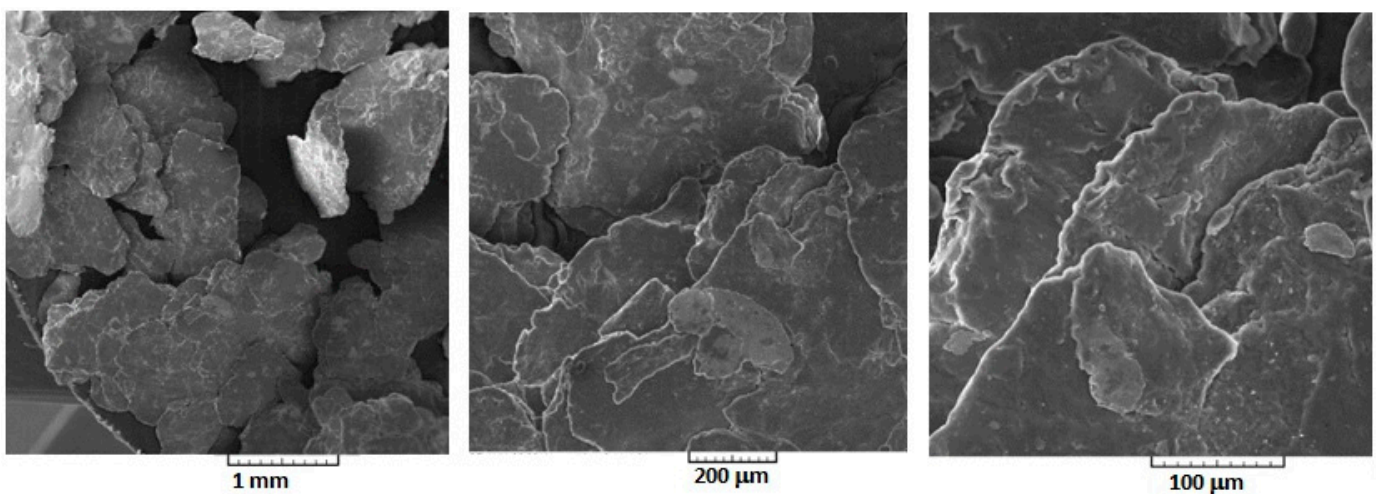


Figure 4. The Mg-10Zn-0.8Ca-0.5Zr (wt.%) alloy-powder processed by mechanical alloying with 200 rpm/6 h/10:1.

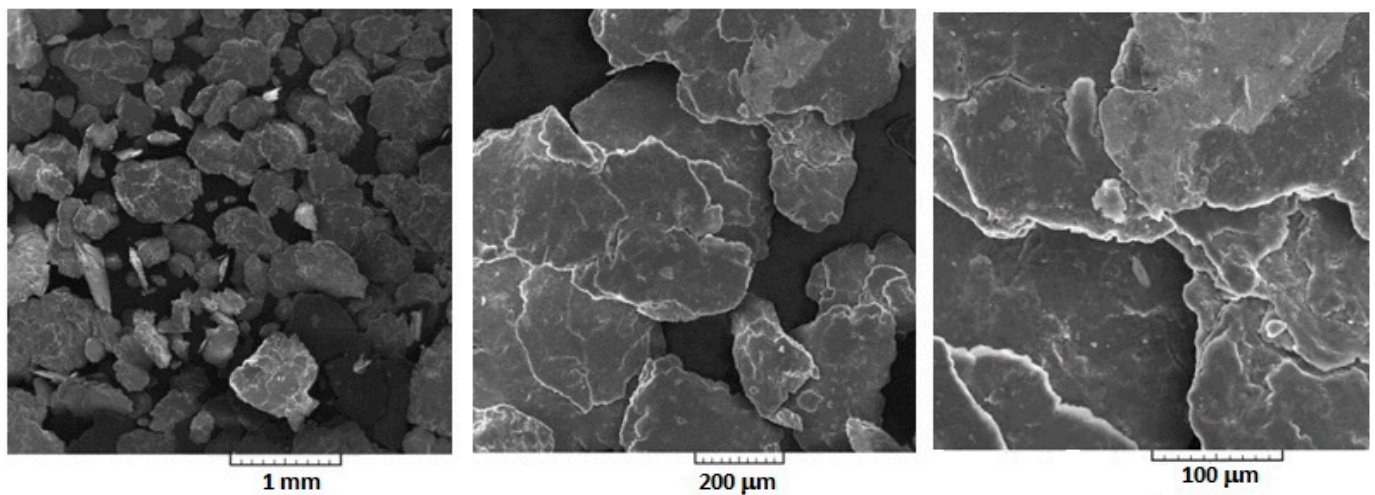


Figure 5. The Mg-10Zn-0.8Ca-0.5Zr (wt.%) alloy-powder processed by mechanical alloying with 200 rpm/20 h/10:1.

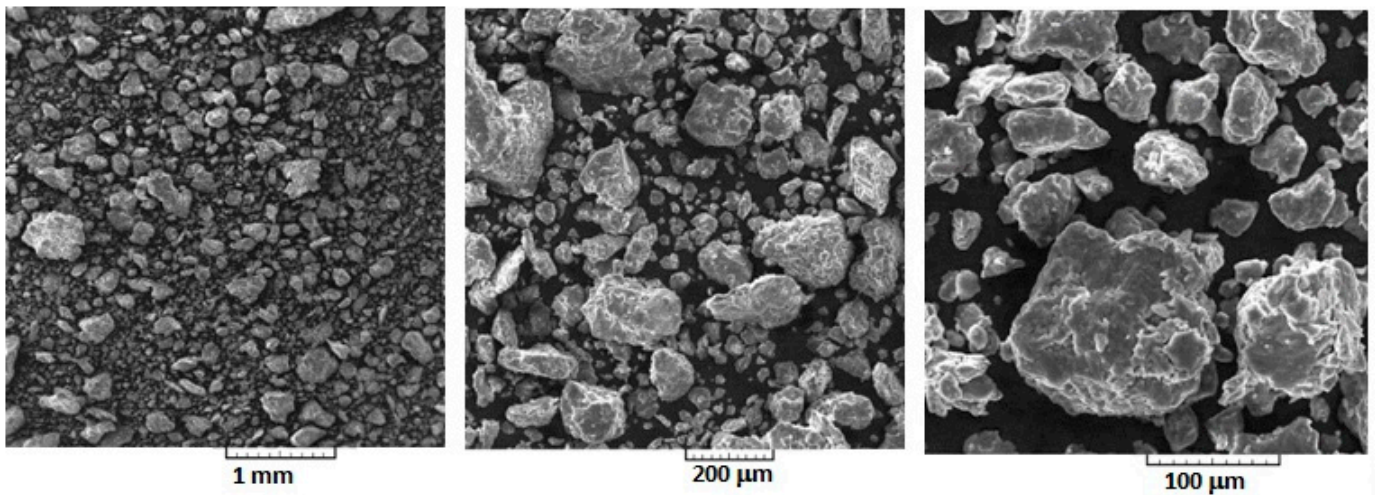


Figure 6. The Mg-10Zn-0.8Ca-0.5Zr (wt.%) alloy-powder processed by mechanical alloying with [200 rpm/24 h/10:1] + [300 rpm/2 h/10:1].

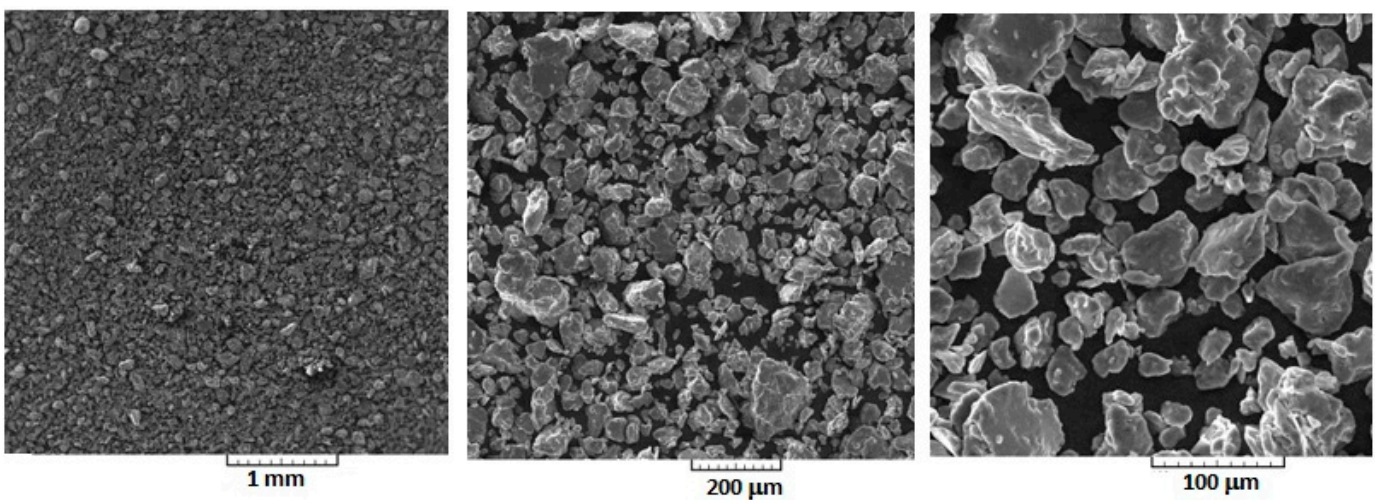


Figure 7. The Mg-10Zn-0.8Ca-0.5Zr (wt.%) alloy-powder processed by mechanical alloying with [200 rpm/24 h/10:1] + [250 rpm/2 h/20:1].

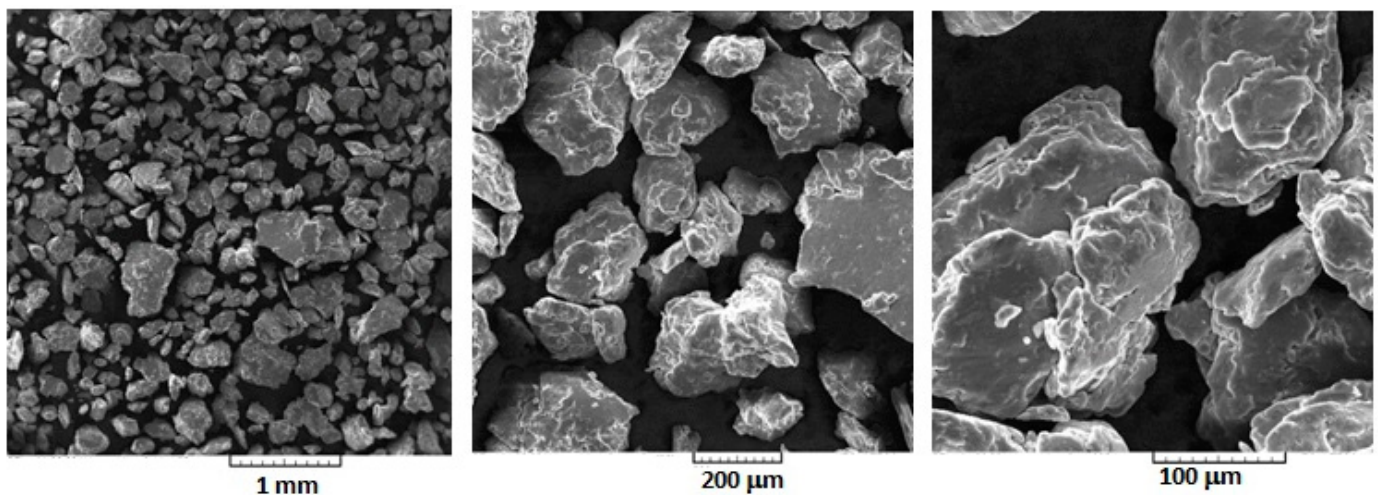


Figure 8. The Mg-10Zn-0.8Ca-0.5Zr (wt.%) alloy-powder processed by mechanical alloying with 300 rpm/16 h/10:1.

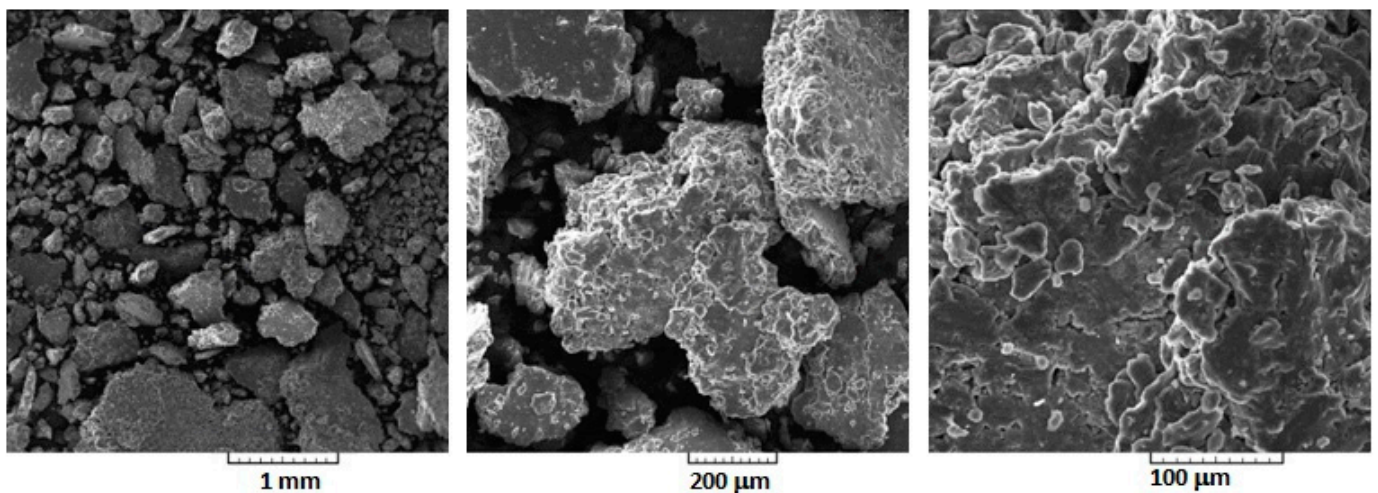


Figure 9. The Mg-10Zn-0.8Ca-0.5Zr (wt.%) alloy-powder processed by mechanical alloying with 300 rpm/28 h/10:1.

The explanation of this process can be summarized as follows: during the mechanical alloying and collision process that takes place, the ratio between the surface area of the mixed intermetallic powders and their volume increases as the severe plastic deformation becomes more accentuated. As a consequence, these powder particles become smaller and smaller by breaking. The hard oxide particles also contribute to the crushing of intermetallic powders. The explanation in the literature for producing the alloying process from various elementary powders and obtaining various types of phases lies in the fact that, during grinding, a very fine mixture of components is formed, most often lamellar in the case of ductile metal powders. Obtaining the alloy itself is mediated by the defects at the level of a crystalline lattice (dislocations, stacking faults, vacancies, etc.) formed in the material as a result of the process of severe cold plastic deformation; these defects have the role of rapid diffusion media while also leading to a slight increase in powder temperature during grinding due to frictional forces and to the impact between the grinding balls or between them and the surface of the container. If the desired structural phase is not obtained directly by mechanical alloying, a short annealing treatment can be applied which favors the diffusion and consequently the formation of the desired final alloy. It follows that by a correct choice of the parameters of the mechanical alloying process but also by choosing an appropriate alloy composition, various alloys can be obtained starting from

metal powders. A special advantage of the mechanical alloying process is the possibility of alloying metals that are difficult or impossible to alloy through classical routes [47,48].

For the present experimental program, the applied mechanical alloying managed to obtain homogeneous alloy powder. Thus, after sieving $<30\ \mu\text{m}$, the obtained powders from the last variants of the experimented scheme (300 rpm/28 h/10:1 for each of three chemical compositions) were subjected to XRD analysis to reveal the constituent phases. The corresponding XRD images (Figure 10) reveal the presence of the majority α -Mg phase, with no other peaks detected, except for the α -Mg phase. This suggests that the milling time was sufficient for Zn, Ca and Zr to be fully soluble in the Mg matrix, which should be the case anyway for the first two compositions, with 4% Zn and 6% Zn, that have an amount of Zn below the maximum solubility of Zn in Mg at ambient temperature. In the case of the third composition, with 10% Zn, even if the solubility limit of Zn in Mg has been exceeded, the detection of the majority phase α -Mg, and only, shows that a supersaturated solid solution was probably obtained, without detected traces of other secondary phases, such as γ -MgZn₂. This fact is also reported in [46], where it is explained that due to the repeated severe plastic deformations of the powder particles cold welded and fractured constantly afterward, the necessary energy is obtained to reach a homogeneous microstructure of the powder particles, with the same composition as a proportion of the starting constituent powders.

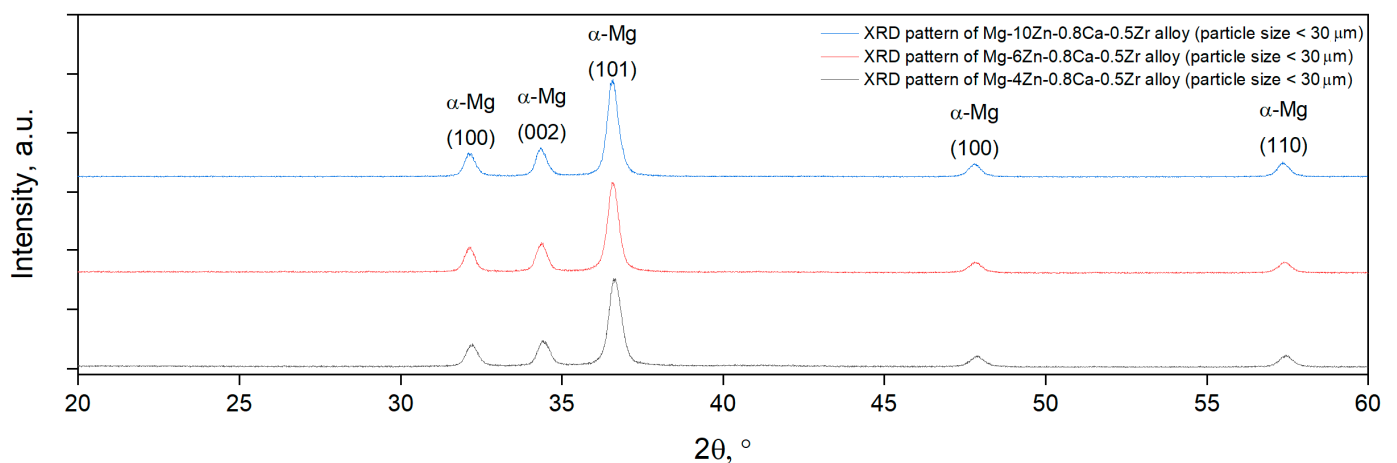


Figure 10. The XRD spectra for all three experimented powder-compositions of Mg-xZn-0.8Ca-0.5Zr (wt.%) alloy (particle size $<30\ \mu\text{m}$).

Together with XRD analysis, an SEM-EDS analysis was performed to certify the obtained chemical composition after the MA process. This analysis was performed on all three tested compositions, but Figure 11 shows only the result for the second tested composition, with 6% Zn, which indicates that the applied MA parameters allowed to obtain the initially selected chemical composition. A similar analysis for the other two compositions also indicates the obtaining of the initially proposed compositions. Compared to the water atomization method, which is known to produce powders with relatively high oxygen content [1,2], the MA method is safer in this respect due to the 1.5 bar argon protective atmosphere of high purity, used for this case. In addition, all auxiliary powder handling operations were performed in a controlled atmosphere. Therefore, oxygen contamination was almost undetectable.

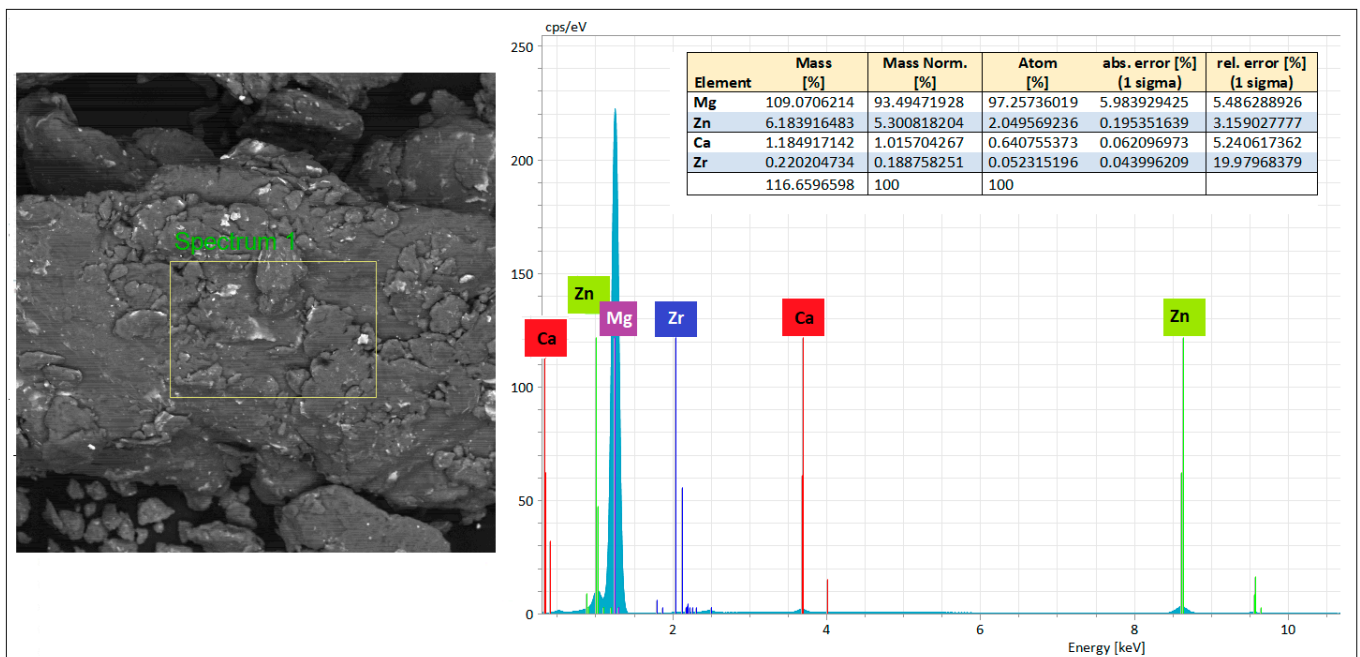


Figure 11. The SEM-EDS image and compositional results for the Mg-6Zn-0.8Ca-0.5Zr alloy after mechanical alloying with 300 rpm/28 h/10:1.

After sieving <math><30\ \mu\text{m}</math>, an SEM analysis was performed for each of three chemical compositions processed with MA parameters: 300 rpm/28 h/10:1. This analysis indicates a direct link between the powder composition and the obtained powder size and shape, for the same milling parameters. On the other hand, for the same composition, the highest experimented milling speed and time conduct to finer powder particles, almost round-shaped, without pores or various inclusions. Thus, Figures 12 and 13 show the SEM images for the Mg powder-alloys with 4% Zn and 10% Zn, respectively. It can be seen that the powder size is more uniform for the case of 10% Zn compared with the other two compositions—a good premise for a promising SLM processing.

Anyway, the most promising results for MA parameters have been certified after applying the SLM technology. In that sense, only for the third experimented composition (Mg-10Zn-0.8Ca-0.5Zr) the SLM sample obtained was robust, non-friable, without cracks and, most important, without balling effect that can be seen for some SLM processed cases, reported in the literature [49]. For the other two tested compositions, the SLM samples were friable. Thus, the MA parameters selected to be suitable for further SLM technology were: 300 rpm/28 h/10:1 for the composition with 10%Zn. Figure 14 shows the macro image of this SLM sample obtained from powder (Mg-10Zn-0.8Ca-0.5Zr) with applied MA parameters: 300 rpm/28 h/10:1. The fact that this MA-powder, obtained and used for the SLM technology with relatively promising results, was not of clear spherical morphology, as is indicated in related literature [46,47] as a must condition, represents a welcome result. Thus, further experiments with a systematic trial for SLM technology will start from this point, from these parameters. It is worth trying/applying a process of atomization as well in inert gases of these new MA-alloys to obtain particles with a spherical shape, or even the use of elemental powders with a spherical shape for the MA process, before SLM experiments.

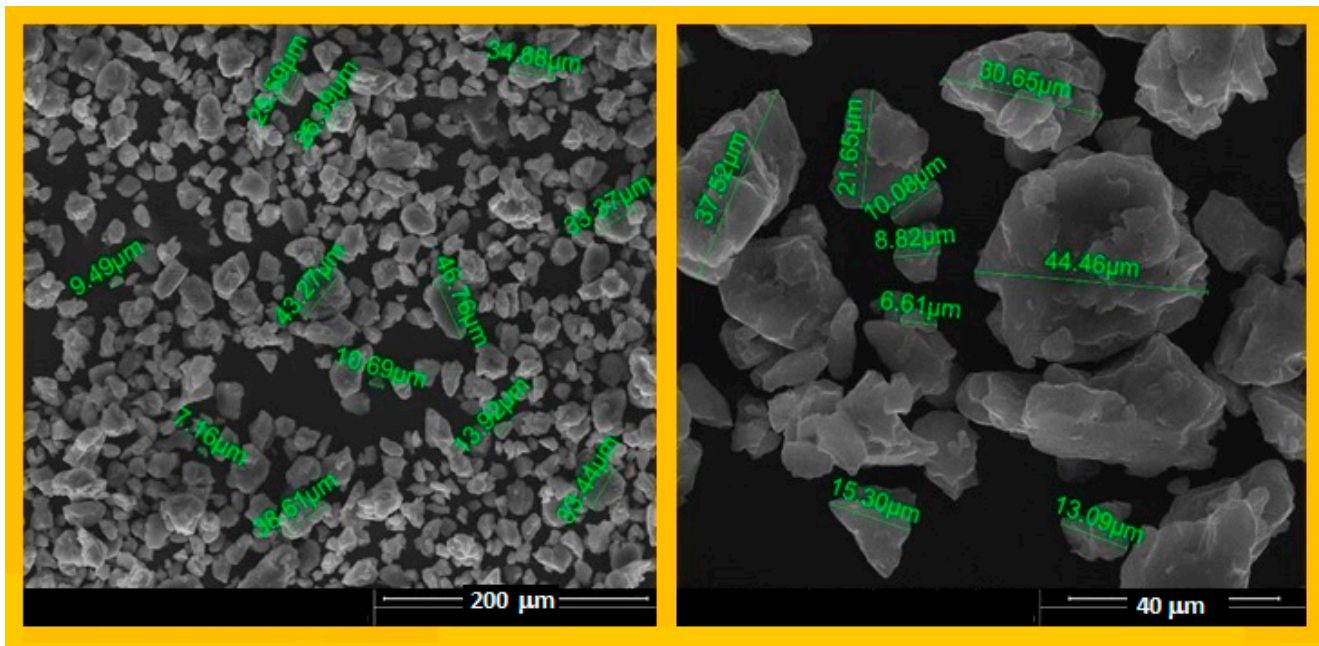


Figure 12. The SEM-SE images for the Mg-4Zn-0.8Ca-0.5Zr alloy after MA with 300 rpm/28 h/10:1 applied parameters and final sieving < 30 μm.

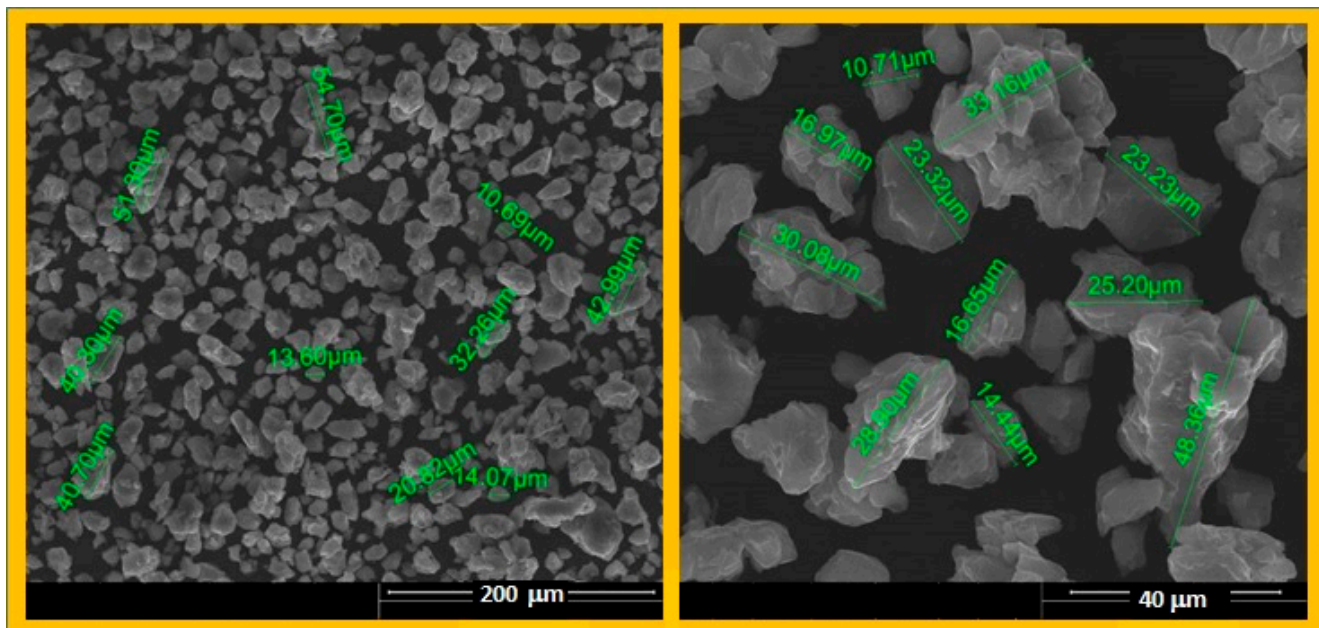


Figure 13. The SEM-SE images for the Mg-10Zn-0.8Ca-0.5Zr alloy after MA with 300 rpm/28 h/10:1 applied parameters and final sieving < 30 μm.



Figure 14. The sample of Mg-10Zn-0.8Ca-0.5Zr alloy-powder processed by SLM—two macro images of the same sample.

4. Conclusions

Three new Mg-based compositions were prepared in the solid state route using mechanical alloying of Mg, Zn, Ca, Zr powder mixture with milling times/milling speed variation: (1) Mg-4Zn-0.8Ca-0.5Zr; (2) Mg-6Zn-0.8Ca-0.5Zr and (3) Mg-10Zn-0.8Ca-0.5Zr.

The morphology of the milled powders reveals fluctuations in the particle size. The fluctuations are characteristic of the MA process because the material is subjected to cold welding, fracturing and grinding.

The MA cyclic process leads to homogeneity in chemical composition (supported by the XRD). The XRD diffraction pattern showed a majority α -Mg solid solution phase for the alloys that were mechanically milled at 28 h and further.

The MA powders with promising results, meaning almost spherical shape, uniform size, without pores or various inclusions, were processed by SLM additive manufacturing technology. The increase of Zn content—from 4 wt.% to 10 wt.%—has a beneficial effect on the sample integrity of the SLM-processed alloys: for the 4 wt.% Zn, the SLM samples show solidification cracking, while for the 10 wt.% Zn, the SLM samples are robust, non-friable and without cracks.

Author Contributions: Conceptualization: D.R., V.D.C. and A.N.; methodology, software: V.D.C.; validation: D.R., V.D.C. and A.N.; formal analysis, investigation, resources: R.H., S.I., D.S., C.T.-R., S.I.D. and E.M.C.; writing—original draft preparation: A.N.; writing—review and editing: D.R., V.D.C. and A.N.; visualization: R.H., S.I., D.S. and C.T.-R.; supervision, project administration: D.R. All authors have read and agreed to the published version of the manuscript.

Funding: This research was funded by Romanian National Authority for Scientific Research, CCCDI-UEFISCDI, Project ERANET-MANUNET-AMMBI/grant no. 207/2020.

Institutional Review Board Statement: Not applicable

Informed Consent Statement: Not applicable

Data Availability Statement: The data presented in this study are available on request from the corresponding author.

Acknowledgments: The authors acknowledge financial support for this research by the Romanian National Authority for Scientific Research CCCDI-UEFISCDI, Project ERANET-MANUNET-AMMBI/grant no. 207/2020.

Conflicts of Interest: The authors declare no conflict of interest.

References

1. Sezer, N.; Evis, Z.; Kayhan, S.M.; Tahmasebifar, A.; Koç, M. Review of magnesium-based biomaterials and their applications. *J. Magnes. Alloy*. **2018**, *6*, 23–43. [[CrossRef](#)]
2. Qin, Y.; Wen, P.; Guo, H.; Xia, D.; Zheng, Y.; Jauer, L.; Poprawe, R.; Voshage, M.; Schleifenbaum, J.H. Additive manufacturing of biodegradable metals: Current research status and future perspectives. *Acta Biomater.* **2019**, *98*, 3–22. [[CrossRef](#)]
3. Staiger, M.P.; Pietak, A.M.; Huadmai, J.; Dias, G. Magnesium and its alloys as orthopedic biomaterials: A review. *Biomaterials* **2006**, *27*, 1728–1734. [[CrossRef](#)]
4. Alvarez, K.; Nakajima, H. Metallic scaffolds for bone regeneration. *Materials* **2009**, *2*, 790–832. [[CrossRef](#)]
5. Manakari, V.; Parande, G.; Gupta, M. Selective Laser Melting of Magnesium and Magnesium Alloy Powders: A Review. *Metals* **2017**, *7*, 2. [[CrossRef](#)]
6. Haude, M.; Ince, H.; Abizaid, A.; Toelg, R.; Lemos, P.A.; Birgelen, C.V.; Christiansen, E.H.; Wijns, W.; Neumann, F.J.; Kaiser, C. Safety and performance of the second-generation drug-eluting absorbable metal scaffold in patients with de-novo coronary artery lesions (BIOSOLVE-II): 6 months results of a prospective, multi centre, non-randomised, first-in-man trial. *Lancet* **2015**, *387*, 31–39. [[CrossRef](#)]
7. Zhao, D.; Witte, F.; Lu, F.; Wang, J.; Qin, L. Current status on clinical applications of magnesium-based orthopaedic implants: A view from clinical translational perspective. *Biomaterials* **2017**, *112*, 287–302. [[CrossRef](#)]
8. Plaass, C.; Von, F.C.; Ettinger, S.; Sonnow, L.; Calderone, F.; Weizbauer, A.; Reifenrath, J.; Claassen, L.; Waizy, H.; Daniilidis, K. Bioabsorbable magnesium versus standard titanium compression screws for fixation of distal metatarsal osteotomies—3 years results of a randomized clinical trial. *J. Orthop. Sci.* **2018**, *23*, 321–327. [[CrossRef](#)] [[PubMed](#)]
9. Lee, J.W.; Han, H.S.; Han, K.J.; Park, J.; Jeon, H.; Ok, M.R.; Seok, H.K.; Ahn, J.P.; Lee, K.E.; Lee, D.H.; et al. Long-term clinical study and multiscale analysis of in vivo biodegradation mechanism of Mg alloy. *Proc. Natl. Acad. Sci. USA* **2016**, *113*, 716–721. [[CrossRef](#)]
10. Zhang, Y.; Xu, J.; Ruan, Y.C.; Yu, M.K.; O’Laughlin, M.; Wise, H.; Chen, D.; Tian, L.; Shi, D.; Wang, J.; et al. Implant-derived magnesium induces local neuronal production of CGRP to improve bone-fracture healing in rats. *Nat. Med.* **2016**, *22*, 1160–1169. [[CrossRef](#)]
11. Yazdimamaghani, M.; Razavi, M.; Vashae, D.; Moharamzadeh, K.; Boccaccini, A.R.; Tayebi, L. Porous magnesium-based scaffolds for tissue engineering. *Mater. Sci. Eng. C Mater. Biol. Appl.* **2017**, *71*, 1253–1266. [[CrossRef](#)]
12. Zhao, L.; Zhang, Z.; Song, Y.; Liu, S.; Qi, Y.; Wang, X.; Wang, Q.; Cui, C. Mechanical properties and in vitro biodegradation of newly developed porous Zn scaffolds for biomedical applications. *Mater. Des.* **2016**, *108*, 136–144. [[CrossRef](#)]
13. Čapek, J.; Vojtěch, D.; Oborná, A. Microstructural and mechanical properties of biodegradable iron foam prepared by powdermetallurgy. *Mater. Des.* **2015**, *83*, 468–482. [[CrossRef](#)]
14. Ljungblad, U. Statistical process control applied to additive manufacturing enables series production of orthopedic implants. *Ann. DAAAM Proc.* **2010**, *21*, 1569–1570.
15. Xilloc.com. The World’s First 3D Printed Total Jaw Reconstruction. Available online: <http://www.xilloc.com/patients/stories/total-mandibular-implant> (accessed on 24 October 2021).
16. Mendoza, H.R. World’s First 3D Printed Vertebrae Are Implanted into Patients in China. 18 August 2014. Available online: <https://3dprint.com/12253/3d-printed-vertebra/> (accessed on 22 October 2021).
17. Ng, C.C.; Savalani, M.M.; Man, H.C.; Gibson, I. Layer manufacturing of magnesium and its alloy structures for future applications. *Virtual Phys. Prototyp.* **2010**, *5*, 13–19. [[CrossRef](#)]
18. Sing, S.L.; An, J.; Yeong, W.Y.; Wiria, F.E. Laser and electron-beam powder-bed additive manufacturing of metallic implants: A review on processes, materials and designs. *J. Orthop. Res.* **2016**, *34*, 369–385. [[CrossRef](#)] [[PubMed](#)]
19. Andani, M.T.; Shayesteh Moghaddam, N.; Haberland, C.; Dean, D.; Miller, M.J.; Elahinia, M. Metals for bone implants. Part1. Powder metallurgy and implant rendering. *Acta Biomater.* **2014**, *10*, 4058–4070. [[CrossRef](#)] [[PubMed](#)]
20. Abbasi, M.; Sajjadi, S.A.; Azadbeh, M. An investigation on the variations occurring during Ni3Al powder formation by mechanical alloying technique. *J. Alloy. Compd.* **2010**, *497*, 171–175. [[CrossRef](#)]
21. Neves, F.; Fernandes, F.M.B.; Martins, I.; Correia, J.B. Parametric optimization of Ti–Ni powder mixtures produced by mechanical alloying. *J. Alloy. Compd.* **2011**, *509*, 271–274. [[CrossRef](#)]
22. Salleh, E.M.; Ramakrishnan, S.; Hussain, Z. Synthesis of Biodegradable Mg–Zn Alloy by Mechanical Alloying: Effect of Milling Time. *Procedia Chem.* **2016**, *19*, 525–530. [[CrossRef](#)]
23. Zheng, Y.F.; Gu, X.N.; Witte, F. Biodegradable metals. *Mat. Sci. Eng. R* **2014**, *77*, 1–34. [[CrossRef](#)]
24. Ng, C.C.; Savalani, M.M.; Lau, M.L.; Man, H.C. Microstructure and mechanical properties of selective laser melted magnesium. *Appl. Surf. Sci.* **2011**, *257*, 7447–7454. [[CrossRef](#)]
25. Zhang, B.; Liao, H.; Coddet, C. Effects of processing parameters on properties of selective laser melting Mg–9%Al powder mixture. *Mater. Des.* **2012**, *34*, 753–758. [[CrossRef](#)]
26. Pawlak, A.; Chlebus, E. Process parameter optimization of Laser Micrometallurgy of AZ31 alloy. *Interdiscip. J. Eng. Sci.* **2015**, *3*, 10–15.
27. Pawlak, A.; Szymczyk, P.E.; Kurzynowski, T.; Chlebus, E. Selective laser melting of magnesium AZ31B alloy powder. *Rapid Prototyp. J.* **2020**, *26*, 249–258. [[CrossRef](#)]

28. Pawlak, A.M.; Rosienkiewicz, E.; Chlebus, E. Design of experiments approach in AZ31 powder selective laser melting process optimization. *Arch. Civ. Mech. Eng.* **2017**, *17*, 9–18. [[CrossRef](#)]
29. He, C.; Bin, S.; Wu, P.; Gao, C.; Feng, P.; Yang, Y.; Liu, L.; Zhou, Y.; Zhao, M.; Yang, S.; et al. Microstructure evolution and biodegradation behavior of laser rapid solidified Mg–Al–Zn Alloy. *Metals* **2017**, *7*, 105. [[CrossRef](#)]
30. Shuai, C.; He, C.; Feng, P.; Guo, W.; Gao, C.; Wu, P.; Yang, Y.; Bin, S. Biodegradation mechanisms of selective laser-melted Mg–xAl–Zn alloy: Grain size and intermetallic phase. *Virtual Phys. Prototyp.* **2017**, *13*, 59–69. [[CrossRef](#)]
31. Shuai, C.; Yang, Y.; Wu, P.; Lin, X.; Liu, Y.; Zhou, Y.; Feng, P.; Liu, X.; Peng, S. Laser rapid solidification improves corrosion behavior of Mg–Zn–Zr alloy. *J. Alloy. Compd.* **2017**, *691*, 961–969. [[CrossRef](#)]
32. Zumdick, N.A.; Jauer, L.; Kersting, L.C.; Kutz, T.N.; Schleifenbaum, J.H.; Zander, D. Additive manufactured WE43 magnesium: A comparative study of the microstructure and mechanical properties with those of powder extruded and as-cast WE43. *Mater. Charact.* **2019**, *147*, 384–397. [[CrossRef](#)]
33. Salehi, M.; Maleksaeedi, S.; Bin Sapari, M.A.; Ling, M.; Nai, S.; Meenashisundaram, G.K.; Gupta, M. Additive manufacturing of magnesium–zinc–zirconium (ZK) alloys via capillary-mediated binderless three-dimensional printing. *Mater. Des.* **2019**, *169*, 107683. [[CrossRef](#)]
34. Lesz, S.; Hrapkiewicz, B.; Karolus, M.; Gołombek, K. Characteristics of the Mg–Zn–Ca–Gd Alloy after Mechanical Alloying. *Materials* **2021**, *14*, 226. [[CrossRef](#)]
35. Bahman, H.; Abdollah, A. Microstructure, mechanical properties, corrosion behavior and cytotoxicity of Mg–Zn–Al–Ca alloys as biodegradable materials. *J. Alloy. Compd.* **2014**, *607*, 1–10.
36. Raducanu, D.; Cojocar, V.D.; Serban, N.; Rusu-Trisca, C.; Necula, M.; Mudrac, R.; Dan, I.; Nocivin, A.; Cinca, I. Processing and properties of a new biodegradable Mg–Zn–Ca–Zr alloy. *Mater. Und Werkst.* **2019**, *50*, 553–564. [[CrossRef](#)]
37. Mostaed, E.; Sikora-Jasinska, M.; Drelich, J.W.; Vedani, M. Zinc-based alloys for degradable vascular stent applications. *Acta Biomater.* **2018**, *71*, 1–23. [[CrossRef](#)] [[PubMed](#)]
38. Levy, G.K.; Goldman, J.; Aghion, E. The Prospects of Zinc as a Structural Material for Biodegradable Implants—A review paper. *Metals* **2017**, *7*, 402. [[CrossRef](#)]
39. Laura, M.P.; Rink, L.; Haase, H. The Essential Toxin: Impact of Zinc on Human Health. *Int. J. Environ. Res. Public Health* **2010**, *7*, 1342–1365.
40. Yang, Y.; Yuan, F.; Gao, C.; Feng, P.; Xue, L.; He, S.; Shuai, C. A combined strategy to enhance the properties of Zn by laser rapid solidification and laser alloying. *J. Mech. Behav. Biomed. Mater.* **2018**, *82*, 51–60. [[CrossRef](#)]
41. Harandi, S.E.; Mirshahi, M.; Koleini, S.; Idris, M.H.; Jafari, H.; Kadir, M.R.A. Effect of Calcium Content on the Microstructure, Hardness and In-Vitro Corrosion Behavior of Biodegradable Mg–Ca Binary Alloy. *Mater. Res.* **2013**, *16*, 11–18. [[CrossRef](#)]
42. Kim, W.C.; Kim, J.G.; Lee, J.Y.; Seok, H.K. Influence of Ca on the corrosion properties of magnesium for biomaterials. *Mater. Lett.* **2008**, *62*, 4146–4148. [[CrossRef](#)]
43. Li, Z.; Gu, X.; Lou, S.; Zheng, Y. The development of binary Mg–Ca alloys for use as biodegradable materials within bone. *Biomaterials* **2008**, *29*, 1329–1344. [[CrossRef](#)]
44. Salahshoor, M.; Guo, Y.B. Surface integrity of biodegradable Magnesium–Calcium orthopedic implant by burnishing. *J. Mech. Behav. Biomed. Mater.* **2011**, *4*, 1888–1904. [[CrossRef](#)]
45. Lee, C.D.; Kang, C.S.; Shin, K.S. Effect of galvanic corrosion between precipitate and matrix on corrosion behavior of as-cast magnesium–aluminum alloys. *Met. Mater. Int.* **2000**, *6*, 351–358. [[CrossRef](#)]
46. Suryanarayana, C. Mechanical Alloying: A Novel Technique to Synthesize Advanced Materials. *Research* **2019**, *2019*, 4219812. [[CrossRef](#)]
47. Ma, E. Alloys created between immiscible metals. *Prog. Mater. Sci.* **2005**, *50*, 413–509. [[CrossRef](#)]
48. Suryanarayana, C.; Liu, J. Processing and characterization of mechanically alloyed immiscible metals. *Int. J. Mater. Res.* **2012**, *103*, 1125–1129. [[CrossRef](#)]
49. Liu, S.; Guo, H. Balling Behavior of Selective Laser Melting (SLM) Magnesium Alloy. *Materials* **2020**, *13*, 3632. [[CrossRef](#)] [[PubMed](#)]